ACS OMEGA

Open Access



http://pubs.acs.org/journal/acsodf

Article

# Research on the Characteristics and Control Technology of Gas Disasters in the Gob of the Nonpillar Working Face Based on the DEM-CFD Coupled Model

Xu Zheng, Shaocheng Ge, Hongwei Liu,* Jia Liu, and Jingjing Yan

Cite This: *ACS Omega* 2024, 9, 3758−3771

Read Online

ACCESS | Metrics & More | Article Recommendations

**ABSTRACT:** Gob-side entry retained by cutting roof (GERCR) is a novel and widely used nonpillar mining technology, but the gas emissions from gob are large, and the gas migration characteristics change obviously, which easily leads to serious safety accidents such as gas explosions and personnel suffocation. The discrete element method-computational fluid dynamics (DEM-CFD) coupled model was proposed and used to study the gas flow field in gob under this technology. Through the calculation of this coupled model, the gas distribution and emission characteristics of gob under different ventilation modes of GERCR technology were clarified, and the areas where the gas exceeds the limit in the roadway were determined. To prevent and control gas accumulation, three-dimensional gas drainage technology in the GERCR working face was proposed based on the above research conclusions. Through the field application and monitoring, the characteristics of gas emission and the effect of gas drainage in the gob of GERCR technology were verified. The on-site monitoring results show that the DEM-CFD coupled model established above can simulate well the gas emission characteristics of the GERCR gob, and the three-dimensional drainage system can well control the gas accumulation in the roadway. The research results are of great significance to control gas disasters of this novel nonpillar mining technology.

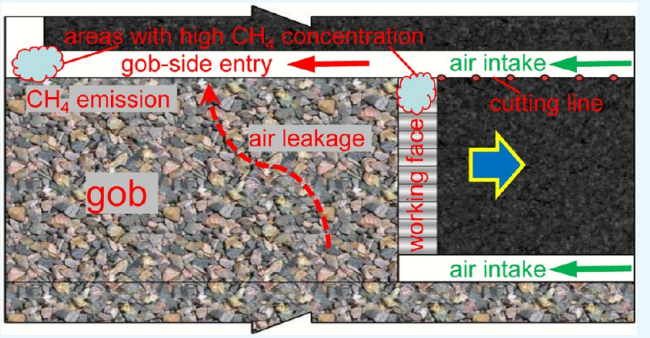


## 1. INTRODUCTION

Gob-side entry retaining (GER) is a popular nonpillar mining technology that has been widely used in United Kingdom, Germany, Poland, Russia, and China since 1950s.[1] This technology can reduce roadway excavation work and increase coal recovery rates.[2,3] However, the stability of filling rock pillars and roadway has been a difficult problem that restricts the popularization of this technology.[4] With the gradual increase of mining depth, the deformation of surrounding rock of retaining roadway is serious, resulting in frequent repair and costly construction.[5−7]

At present, this technology usually uses a roadside filling method to maintain and retain the original mining roadway along the edge of gob,[8,9] thus canceling the roadway protective coal pillar, and using the roadway retained along gob as the mining roadway of the next panel. In recent years, a new nonpillar mining technology, gob-side entry retaining by cutting roof (GERCR), has been put forward by a Chinese scientific research team.[10,11] The differences between the GERCR mining method and other longwall mining methods are shown in Figure 1. In this technology, the relationship between the gob roof and the entry roof is cut off using a directional joint-cutting technique, forming a short cantilever beam structure above the entry roof. This avoids the violent effects of entry surrounding rocks induced by caving and movement of superficial roof strata above the gob. In addition, it can also make full use of the caved rocks' broken expansion characteristics and form a support structure for the upper main roof, thereby reaching the aim of removing the coal pillar or backfilling body. However, the treatment of gob gas is the main problem in mining by using GERCR technology. As one side of the retaining roadway is the caved zone of gob, gob is exposed to the airflow, forming a completely open state. Compared with the closed gob condition of the traditional mining technology, the gob is not closed, the air leakage is serious, and the gas in gob can easily leak into the roadway under the negative pressure. Gas in the roadway exceeds the limit extremely easily, which leads to major safety accidents such as gas explosions and seriously threatens the safety of

Received: October 6, 2023
Revised: December 8, 2023
Accepted: December 14, 2023
Published: January 12, 2024

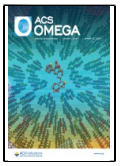

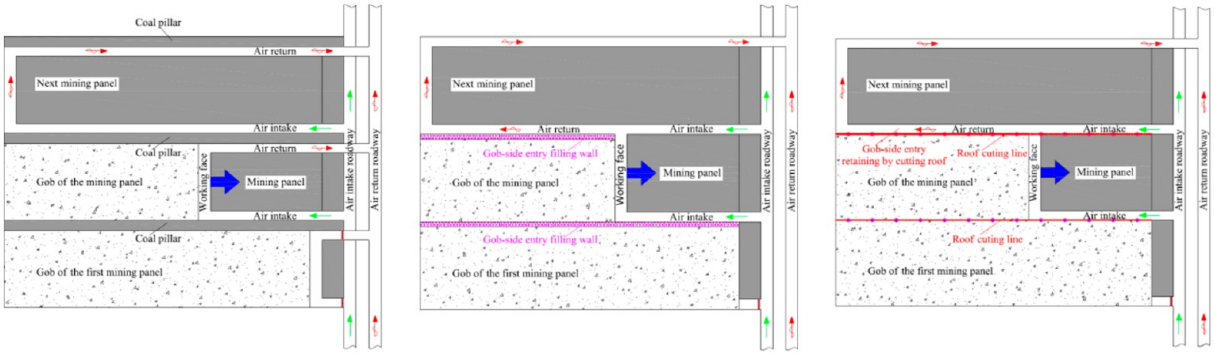


(a) Longwall mining with coal pillar

(b) Traditional gob-side entry longwall mining method

(b) GERCR longwall mining method

**Figure 1.** (a−c) Longwall mining methods with coal pillar and without coal pillar.

workers and mine production.[12−14] During the process of mining by using GERCR technology, the overburden collapse and fracture development in gobs are very different from the traditional mining method, which results in corresponding changes of the air leakage mode and the gas drainage mode in gob. At the same time, with the increase of the coal mining scale and depth in China,[15] the gas content and gas emission gradually increase.[16] All of these have increased the difficulty of gas control in mining by the use of GERCR technology. Thus, this technology is only applied and popularized in a thin or medium thick coal seam with low gas emission in China now.

The explosion concentration of gas is 5−15%, so it must be strictly controlled in coal mining, and the maximum concentration restricted in the working face is 1% in China. Mine ventilation[17,18] and gas drainage[16,19,20] are two ways to control gas emission. However, the characteristics of gas emission in the gob under different ventilation types in the GERCR working face are not clear by now, and accordingly, no effective gas drainage mode in the gob under this condition has been determined. The study of the above problems will inevitably involve the definition of the gob medium and the analysis of the gas flow field in it. At present, researchers generally regard the gob of the longwall working face as a porous medium. The gas emission and flow in the gob of the longwall working face are controlled by many variables, including the characteristics of gob (such as permeability and porosity),[21] source term of gas emission,[22] ventilation mode and parameters,[23,24] gas drainage mode and parameters,[25,26] etc. Computational fluid dynamics (CFD) numerical simulation technology is an important method to study the dynamic characteristics of the gob flow field, and a lot of the noted results have been achieved by this technology.[27,28] In the process of simulating gob gas flow by CFD, porosity and permeability of gob porous medium are the two important key parameters, and they are obtained by studying overburden collapse and fracture development.[25,29,30] In previous studies, the overburden strata are generally classified into a caved zone, fractured zone, and continuous deformation zone.[31−33] There is an annular overlying fracture zone in gob which provides a good accumulation zone and channel for gas migration.[33−35] The research methods of overburden collapse and fracture development in gob mainly include theoretical analysis,[36] empirical statistics,[37] numerical simulation,[38,39] similar simulation,[40] and field measurement.[41] DEM (discrete element method) numerical simulation can intuitively reflect different geological and mining processes, get detailed parameters such as stress, fracture, and porosity, and provide a scientific basis for the study of the flow field in gob. Thus, it is a commonly used method to study overburden collapse and fracture development in gob.

Under the conditions of mining by using GERCR technology, the overburden collapse and fracture development in gob is obviously different from that of the traditional longwall mining method. In order to conduct scientific research on the gas flow field in gob, this paper first used DEM software to study the overburden collapse and fracture development in gob under the condition of GERCR. Through DEM numerical simulation, the spatial distribution of porosity in gob was obtained directly, and then the spatial distribution of permeability was obtained by the relationship between porosity and permeability.[42] After that, through the UDF function of CFD numerical simulation, the corresponding porosity and permeability were introduced into the calculation of the gas flow field in the gob, so as to obtain the characteristics of gas emission in the gob under the condition of mining by using GERCR technology. According to the characteristics of gas emissions in gob, effective control technology was put forward to realize safe production of coal mining and comprehensive utilization of gas. After that, through field application and long-term monitoring, the characteristics of gas emissions and the effect of gas drainage in the gob of GERCR technology were verified.

## 2. GERCR ENGINEERING BACKGROUND

China is the largest coal producing and consuming country in the world, and Shanxi is one of the most important coal producing provinces in China. The Duerping coal mine is located in the northwest of the Xishan coalfield, Shanxi Province, China, 15 km away from Taiyuan City. The mine area is 69.7666 km$^2$. The Duerping coal mine has an annual production capacity of 5 million tons. According to statistics, the annual loss of coal due to the isolation of coal pillars along the roadway can reach 100,000 tons, which causes a serious waste of resources and huge economic losses. In addition, the section coal pillar will become the peak area of mine pressure, and the mine pressure appears obviously, which also poses a certain threat to the safety of the roadway. Since 2017, the GERCR nonpillar mining technology has been experimented in the working face 62711 of #2 coal seam. The thickness of



https://doi.org/10.1021/acsomega.3c07755
ACS Omega 2024, 9, 3758−3771

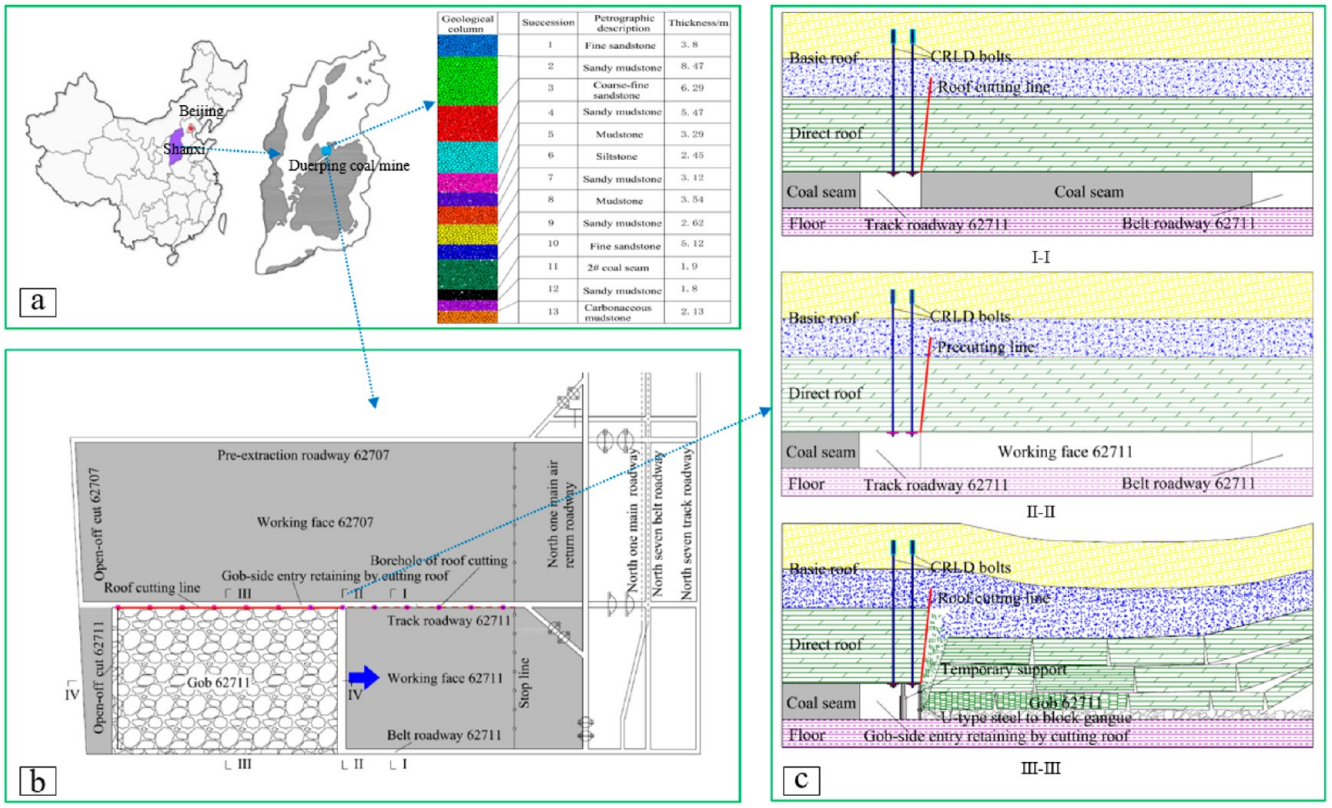


**Figure 2.** Field application of GERCR technology. (a) Geographical location and geological conditions of working face 62711; (b) underground construction drawings of working face 62711 mining by GERCR technology; (c) profile of the GERCR mining process of working face 62711.

the coal seam is stable, and the structure is simple. The coal thickness is 1.00−2.40 m, with an average of 1.90 m. The coal seam dip is 1−7 degrees, with an average of 2 degrees. The length of working face is 216 m, the strike length is 1564 m, and the average mining height is 1.90 m. The location of the roof cutting roadway is track roadway 62711, the length of the roof cutting roadway is 1564 m, and the depth of the cutting line is 6 m. The specific gas emission and gas production rate of the whole mine are 21.41 $m^3/t$ and 188.06 $m^3/min$, respectively. The specific gas emission and gas production rate of the working face are 15.64 $m^3/t$ and 20 $m^3/min$, respectively. The field application of GERCR technology in working face 62711 is shown in Figure 2. The construction process of GERCR nonpillar mining technology in working face 62711 is as follows: (1) After the formation of track roadway 62711 and belt roadway 62711, constant resistance and large deformation bolts (CRLD) were constructed on the roof of track roadway 62711. (2) The boreholes of roof cutting were constructed at a distance not less than 50 m ahead of the working face. (3) Along the advance direction of working face 62711, precutting blasting was carried out successively with special equipment to form a precutting line. (4) Advance the working face. (5) Temporary reinforcement support and temporary intensive gangue retaining support were carried out in time after the working face was advanced. (6) With the advance of the working face, the roof continuously collapsed. After the collapsed roof was stable, the temporary monomer pillars were withdrawn, and the air-leakage material was sprayed on the side of the roadway of roof cutting.

## 3. GAS EMISSION CHARACTERISTICS OF GERCR GOB

**3.1. Overburden Collapse and Fracture Development.** PFC (particle flow code) is numerical simulation software developed by Itasca Company in the United States. At present, this software is mainly used in the research of granular materials, which belongs to the field of DEM numerical simulation. The materials generated by PFC numerical simulation can be separated and broken under stress conditions, so as to simulate the process of overburden collapse and fracture development.[43−45] According to the actual situation of the GERCR working face in the Duerping mine (as shown in Figure 2), the PFC2D model was established along the strike and dip direction of the working face respectively to simulate the overburden collapse and fracture development of the GERCR gob.

In the process of PFC numerical simulation of the rock damage mechanism, the parallel-bond model was selected as the constitutive model. In addition, it is necessary to use the mesoscopic parameters of the particles to characterize the rocks. However, these mesoscopic parameters are different from the macroscopic parameters of rocks, which need to be scientifically transformed. The mesoscopic parameters of model particles mainly include contact modulus $E_c$, contact stiffness ratio $k_n/k_s$, and friction coefficient $f$. The mesoscopic parameters of the parallel-bond model mainly include the parallel-bond radius multiplier $\lambda$ (set to 1 uniformly), the bond modulus $\overline{E_c}$, the ratio of bond normal and bond shear stiffness $\overline{k_n}/\overline{k_s}$, the bond tensile strength $\overline{\sigma}$, and the bond shear strength $\overline{\tau}$. Due to the large number of mesoscopic parameters involved in the parallel-bond model, in order to simplify the research process, the following assumptions can be made in the


https://doi.org/10.1021/acsomega.3c07755
ACS Omega 2024, 9, 3758−3771

Table 1. Macro-Mesoscopic Parameters of the Overburden in Working Face 62711 of the Duerping Mine

| succession | petrographic description | thickness/m | density/kg·m$^{-3}$ | $E_c$/10$^9$Pa | $k_n/k_s$ | $f$ | $\overline{E}_c$/10$^9$Pa | $\overline{k}_n/\overline{k}_s$ | $\overline{\sigma}$ /10$^6$ Pa | $\overline{c}$ /10$^6$ Pa | $\overline{\varphi}$ /° |
|---|---|---|---|---|---|---|---|---|---|---|---|
| 1 | Fine sandstone | 3.8 | 2653 | 5.4 | 1.56 | 0.7 | 5.4 | 1.56 | 8.51 | 10.87 | 39.1 |
| 2 | Sandy mudstone | 8.47 | 2462 | 4.06 | 1.37 | 0.5 | 4.06 | 1.37 | 6.41 | 6.12 | 34.2 |
| 3 | Coarse-fine sandstone | 6.29 | 2510 | 6.1 | 1.74 | 0.7 | 6.1 | 1.74 | 7.14 | 6.84 | 39.5 |
| 4 | Sandy mudstone | 5.47 | 2435 | 3.32 | 1.39 | 0.3 | 3.32 | 1.39 | 4.26 | 4.52 | 34.2 |
| 5 | Mudstone | 3.29 | 2315 | 2.08 | 1.28 | 0.5 | 2.08 | 1.28 | 3.53 | 4.82 | 34.9 |
| 6 | Siltstone | 2.45 | 2620 | 6.3 | 1.29 | 0.8 | 6.3 | 1.29 | 7.06 | 10.25 | 38.4 |
| 7 | Sandy mudstone | 3.12 | 2462 | 3.3 | 1.37 | 0.5 | 3.3 | 1.37 | 4.41 | 4.08 | 34.2 |
| 8 | Mudstone | 3.54 | 2230 | 2.04 | 1.21 | 0.4 | 2.04 | 1.21 | 3.82 | 4.15 | 30.9 |
| 9 | Sandy mudstone | 2.62 | 2500 | 3.82 | 1.2 | 0.4 | 3.82 | 1.2 | 7.69 | 8.5 | 31.6 |
| 10 | Fine sandstone | 5.12 | 2637 | 3.35 | 1.17 | 0.5 | 3.35 | 1.17 | 6.65 | 6.98 | 32.2 |
| 11 | #2 coal seam | 1.9 | 1350 | 2.19 | 2.09 | 0.4 | 2.19 | 2.09 | 5.1 | 4.26 | 40.8 |
| 12 | Sandy mudstone | 1.8 | 2520 | 4.54 | 1.3 | 0.3 | 4.54 | 1.3 | 7.9 | 8.7 | 36.3 |
| 13 | Carbonaceous mudstone | 2.13 | 2510 | 3.43 | 1.45 | 0.3 | 3.43 | 1.45 | 7.29 | 6.86 | 36.9 |

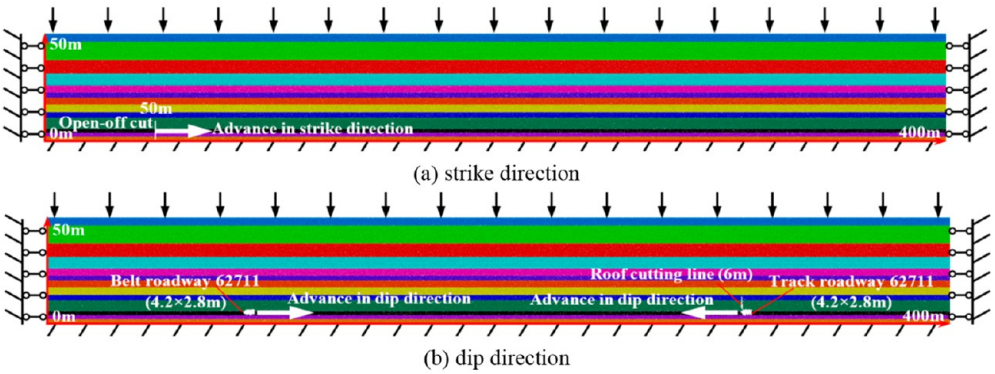


**Figure 3.** (a, b) PFC model of the 62711 GERCR working face in the Duerping coal mine.

research:[46] (1) Because the friction coefficients of the macroscopic model and the mesoscopic model are similar, it is assumed that they are equal in the numerical calculation. (2) Considering the homogeneity of the test sample, it is assumed that the contact modulus and the bond modulus of the particles are equal; that is, $E_c = \overline{E}_c$; the contact stiffness ratio and the ratio of bond normal and bond shear stiffness are equal, that is, $k_n/k_s = \overline{k}_n/\overline{k}_s$. (3) Because the PFC model uses round particles, the cohesion of the model is larger than the actual coal and rock mass, and the internal friction angle is smaller than the actual coal and rock mass;[47,48] therefore, the mesoscopic parameters cohesion $\overline{c}$ and internal friction angle $\overline{\varphi}$ are used to replace the shear strength in the numerical calculation, and the parameters are equal to the cohesion and internal friction angle in the macroscopic parameters. In order to obtain the relationship between macroscopic parameters and mesoscopic parameters, researchers have conducted regression analysis on the correlation between them through a large number of indoor physical experiments and numerical simulations, and obtained the empirical eqs 1−4 between them.[38,49]

$$E/E_c = a + b\ln(k_n/k_s) \tag{1}$$

$$\nu = c\ln(k_n/k_s) + d \tag{2}$$

$$\frac{\sigma_c}{\overline{\sigma}} = \begin{cases} d\left(\frac{\overline{\tau}}{\overline{\sigma}}\right)^2 + e\frac{\overline{\tau}}{\overline{\sigma}}, & 0 < \frac{\overline{\tau}}{\overline{\sigma}} \le 1 \\ f, & \frac{\overline{\tau}}{\overline{\sigma}} > 1 \end{cases} \tag{3}$$

$$\frac{\sigma_t}{\overline{\sigma}} = \begin{cases} h\left(\frac{\overline{\tau}}{\overline{\sigma}}\right)^2 + i\frac{\overline{\tau}}{\overline{\sigma}}, & 0 < \frac{\overline{\tau}}{\overline{\sigma}} \le 1 \\ j, & \frac{\overline{\tau}}{\overline{\sigma}} > 1 \end{cases} \tag{4}$$

where $E$ is elastic modulus, GPa; $\nu$ is Poisson's ratio; $a$ = 1.652; $b$ = −0.395; $c$ = 0.209; $d$ = 0.111; $\sigma_c$ is the compressive strength, MPa; $\overline{\sigma}$ is the bond tensile strength, MPa; $\overline{\tau}$ is the bond shear strength, MPa; $d$ = −0.965; $e$ = 2.292; $f$ = 1.327; $\sigma_t$ is the tensile strength, MPa; $h$ = −0.174; $i$ = 0.463; $j$ = 0.289.

By using eqs 1−4, the required mesoscopic parameters were obtained on the basis of the macroscopic parameters of the strata. After that, the mesoscopic parameters were modified repeatedly by a trial and error method until the macroscopic mechanical parameters expressed by the numerical simulation experiment were consistent with the indoor physical experiment. The main mesoscopic parameters of the overburden of working face 62711 of the Duerping mine are shown in Table 1. The PFC2D model was established along strike sections IV−IV and dip sections III−III of working face 62711 in Figure 2. Both of the model dimensions were 50 m (height) × 400 m (width), and the vertical loading stress of the model was 12.593 MPa. According to the geologic column of working face 62711 in Figure 2, a total of 13 layers of coal and rock were generated, and the macro-mesoscopic parameters of each layer were shown in Table 1. The dip angle of the model was 0°, the particle radius was 0.2−0.3 m, and the original porosity of the generated model was 0.01. The width of working face was 216 m, the width × height of belt roadway and track roadway were 4.2 × 2.8 m, the cutting height of the roof was 6 m (the cutting



https://doi.org/10.1021/acsomega.3c07755
ACS Omega 2024, 9, 3758−3771

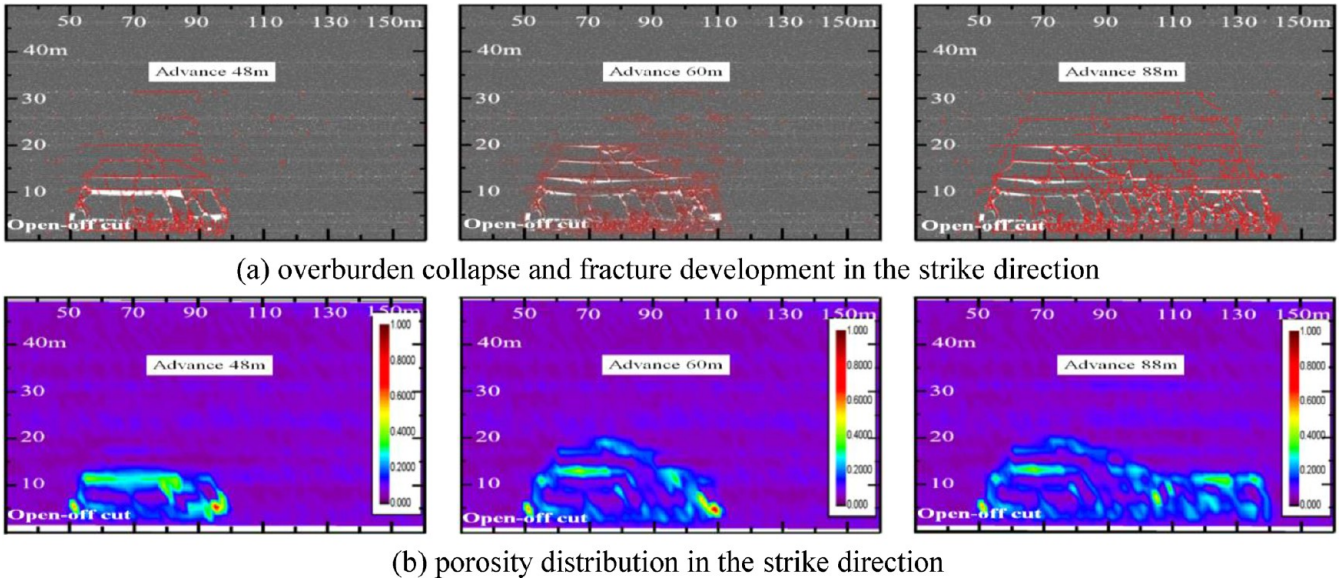


**Figure 4.** (a, b) Overburden collapse, fracture development, and porosity distribution in the strike direction.

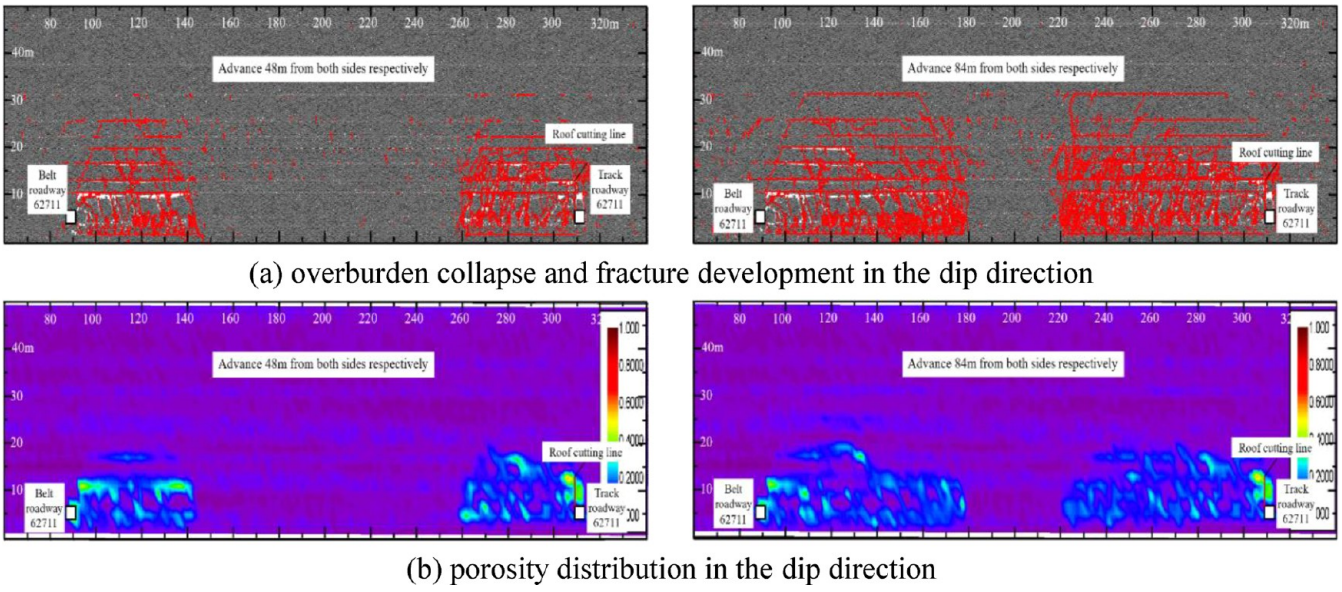


**Figure 5.** (a, b) Overburden collapse, fracture development, and porosity distribution in the dip direction.

line was vertical to the roof, ignoring the smaller deflection angle from the vertical direction), and the thickness of coal seam was 1.9 m. The strike direction was gradually excavated along the open-off cut, and the dip direction was alternately excavated along the belt roadway and the track roadway, as shown in Figure 3.

In the process of mining by using GERCR technology, the collapse and fracture development of gob overburden were calculated by the PFC simulation models shown in Figure 3, and the overburden collapse, fracture development, and porosity change in the strike and dip direction are shown in Figure 4 and Figure 5, respectively.

(1) Destruction and collapse of overburden. As shown in Figure 4 and Figure 5, in the advance process of working face 62711, the direct roof of #10 fine sandstone began to collapse gradually with the increase of the advance distance, the basic roof of #9 sandy mudstone had its first destruction when the working face was advanced to 48 m, #8 mudstone and #7 sandy mudstone collapsed with the initial break of #9 sandy mudstone. According to the key layer theory proposed by Chinese scholars Qian and others,[50] #9 sandy mudstone was the first subkey layer. With the continuous advance of the working face, #6 siltstone showed obvious damage and subsidence, and #5 mudstone and #4 sandy mudstone collapsed with the collapse of # 6 siltstone, indicating that #6 siltstone was the second subkey layer. After the working face was advanced to 88 m, the #4−10 layers collapsed completely, and obvious stratification appeared between #4 and #3 layers. After that, with the further advance of the working face, no obvious destruction occurred in #3 coarse-fine sandstone and the layers above it, indicating that #3 coarse-fine sandstone was the main key layer. The overburden of gob broke and collapsed periodically under the main key layer. The collapse law of overburden on the roof cutting side was



https://doi.org/10.1021/acsomega.3c07755
ACS Omega 2024, 9, 3758−3771

obviously different from that on the roof not cutting side. The cutting line cut off the basic roof. Along the strike direction, with the advance of the working face, the direct roof (#10 fine sandstone), basic roof (# 9 sandy mudstone), #8 mudstone and #7 sandy mudstone collapsed at the same time. The overburden above the first subkey layer collapsed in time at the early stage of working face advance, and the rocks were sufficiently broken, which played a certain supporting role on the overburden. With the increase of strike advance distance, the second subkey layer (#6 siltstone) on the roof cutting side broke and collapsed, and the #5 mudstone and #4 sandy mudstone collapsed with the collapse of #6 siltstone. The overburden on the roof cutting side also eventually collapsed to the main key layer (#3 coarse-fine sandstone). The broken swelling degree of the collapsed rocks on the roof cutting side was greater than that on the roof not cutting side.

(2) Fracture development of overburden. In the process of mining, the overburden in gob will form horizontal separation fracture and vertical broken fracture. The horizontal separation fracture is the fracture along the layer formed between layers with the subsidence of the strata. It causes the coal seam to expand and deform, so that the gas pressure is released, and the gas flows out along the separation fracture. The broken fracture is formed with the break and subsidence of the layers, which connects the gas channel between the upper and lower layers.[50] As shown in Figure 4 and Figure 5, with the advance of the working face, the separation fracture and broken fracture gradually developed, and the key layer played an important role in the development of the fracture. In the upper part of coal seam and the lower part of main key layer, the separation fracture and broken fracture developed at the same time. In the upper part of the main key layer, the broken fracture no longer developed, and the separation fracture only developed in a small range. The development law of the overburden fracture on the roof cutting side was obviously different from that on the roof not cutting side. The fracture on the roof cutting side developed sufficiently at the early stage of the advance in the dip direction, and then with the collapse of the basic roof, the development degree of the fracture began to decrease. In the range from the upper part of coal seam to the basic roof, the development degree of fracture on the roof cutting side was higher; in the range from the upper part of the basic roof to the main key layer, the development degree of fracture on the roof not cutting side was higher.

(3) Change of overburden porosity. With the advance of the working face, a large area of gob is left behind, which is composed of broken coal and rock, and the porosity is an important parameter to study the air leakage flow field in the whole gob. At present, the flow field simulation of gob is mostly based on the self-defined porosity model,[21] and the results are not in good agreement with the field. To solve this problem, the porosity data collected in the PFC simulation were used to analyze the change rule of porosity with the advance of the working face. With the advance of the working face, the porosity changed constantly, and the porosity in the range of separation layer was significantly higher than that in other areas. The area where the porosity changed obviously was consistent with the caved zone, and the porosity in the fracture zone had no significant change. With the advance of the working face, the porosity of the same location changed with time. The above phenomena show that the change of porosity is a function of space and time, and the separation (broken)-compaction-closure process of overburden in gob has an important influence on porosity. In the dip direction, the porosity on the roof cutting side changed greatly in the early stage of excavation. On the roof not cutting side, with the complete collapse of the basic roof, the porosity began to change obviously. When the extraction was completed in the dip direction, the area where the overburden porosity increased significantly on the roof cutting side was smaller than that on the roof not cutting side, indicating that the gob on the roof cutting side was more unfavorable to gas flow.

**3.2. DEM-CFD Coupled Model.** In the mining process, the stress distribution changes, the overburden subsidence, deformation and collapse occur, forming the caved zone, fractured zone, and continuous deformation zone in the gob.[31−33] The caved zone and fractured zone provide a channel for gas flow. In the process of studying the gas flow in gob, these zones can be regarded as porous medium, and the difficulty of gas passing through is determined by the porosity and permeability.[21] Thus, it is necessary to get the correct porosity and permeability distribution in gob before using the CFD to calculate the gas flow. The empirical equations are often used to define the flow resistance of the porous medium in the gob. Essentially, the porous medium model adds a source term representing momentum consumption to the momentum equation (as shown in eq 5). The source term consists of the viscous resistance term and inertial resistance term.

$$S_i = -\left(\sum_{j=1}^{3} D_{ij}\mu v_j + \sum_{j=1}^{3} C_{ij}\frac{1}{2}\rho|v_j|v_j\right) \tag{5}$$

where $S_i$ is the source term in the $i$th ($x$, $y$, or $z$ direction) momentum equation; $D_{ij}$ and $C_{ij}$ are the resistance coefficient matrices of viscosity and inertial, respectively; $\mu$ is the dynamic viscosity of gob mixture gas; $v_j$ is the component of velocity in the $j$ direction. In a simple and uniform porous medium, the following mathematical model can also be used:

$$S_i = -\left(\frac{\mu}{k}v_i + C_2\frac{1}{2}\rho|v_j|v_j\right) \tag{6}$$

where $k$ is the permeability, and $\frac{1}{k}$ and $C_2$ are defined as the viscous resistance coefficient and inertial resistance coefficient.

In turbulent flow, there is viscous resistance and inertial resistance in the flow medium. Under this condition, the semiempirical eq 7 is often used to calculate the correlation.

$$\nabla p = \frac{150\mu(1-\varepsilon)^2}{D_p^2\varepsilon^3}\nu + \frac{1.75\rho(1-\varepsilon)}{D_p\varepsilon^3}V\nu \tag{7}$$

where $D_p$ is the average particle diameter, m; $\varepsilon$ is the fraction of space, that is, the volume of space (excluding the original pores) divided by the total volume, which can be defined as the porosity in gob.

In laminar flow through a porous medium, the pressure drop is proportional to the velocity, and the constant $C_2$ can be set



https://doi.org/10.1021/acsomega.3c07755
ACS Omega 2024, 9, 3758−3771

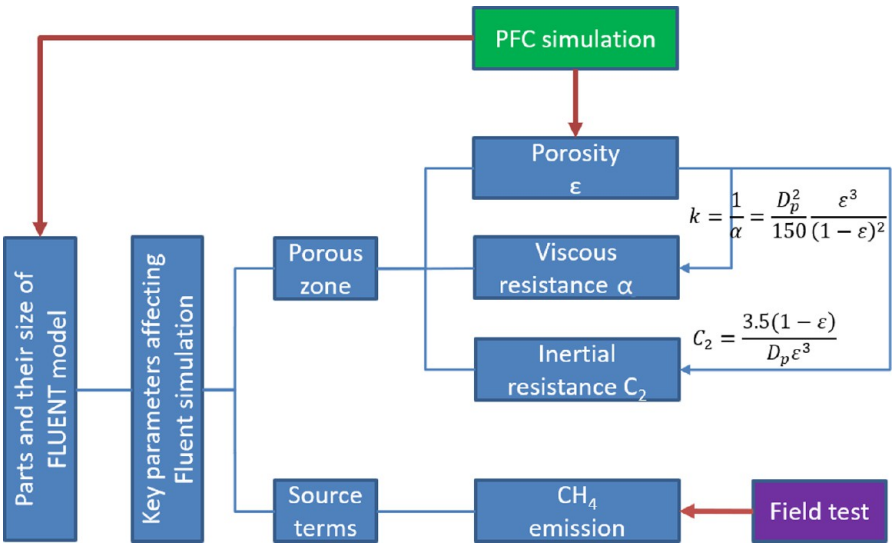


**Figure 6.** Flowchart of numerical simulation of the flow field in gob of mining with gob-side entry formed by cutting roof based on the DEM-CFD coupled model.

to 0. Neglecting the convection acceleration and diffusion term, the flow in porous medium can be simplified to Darcy's Law: $\nabla p = -\frac{\mu}{k}\nu$. Thus, in the process of simulation of gas flow in gob, it is important to study the permeability in gob, and it can be estimated by using the Blake-Kozeny equation.

$$k = \frac{1}{\alpha} = \frac{D_p^2}{150}\frac{\varepsilon^3}{(1-\varepsilon)^2} \tag{8}$$

In turbulent flow, in addition to the viscous resistance, the inertial resistance can be obtained from eq 9:

$$C_2 = \frac{3.5(1-\varepsilon)}{D_p\varepsilon^3} \tag{9}$$

In this paper, the DEM-CFD coupled model was put forward, and the working flowchart of the model is shown in Figure 6. According to the above PFC numerical simulation results, the range of caved zone and fractured zone was determined first. Then, the spatial distribution of porosity in gob was obtained directly, and the spatial distribution of permeability was obtained through eq 8. After that, through the UDF function of FLUENT (a commonly used CFD numerical simulation software), the corresponding porosity and permeability were introduced into the calculation of the gas flow field in the gob, so as to obtain the characteristics of gas emission in the gob under the conditions of mining by using GERCR technology. According to PFC simulation results as shown in Figure 4 and Figure 5, the height of the caving zone and fracture zone of working face 62711 were 16.3 m and 11.21 m, respectively (shown in Figure 7). The direct roof and basic roof were cut off by using the GERCR technology, thus increasing the height of the caving zone, reducing or even eliminating the hole and fracture channels formed by the support of the coal pillar near the roadway. After the roof above the roadways on both sides of the working face was cut off, the caved zone can be divided into the separation zone near open-off cut, fully caved zone formed by cutting roof, and separation zone near working face (shown in Figure 8). Based on the results of PFC numerical simulation, the distribution equations of porosity in the gob of the above-mentioned different zones were obtained by fitting, and the equations are shown in eqs 10−12, and the porosity distribution diagram is shown in Figure 9.

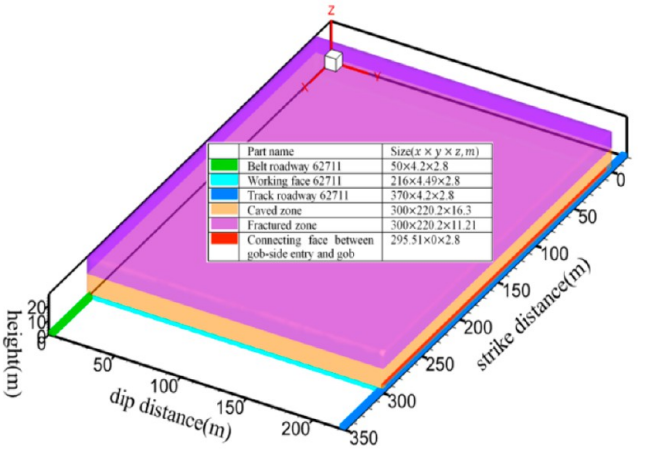


**Figure 7.** Parts and their sizes of the FLUENT simulation model.

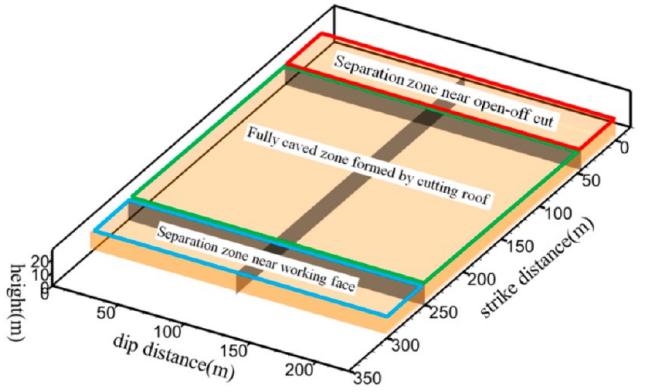


**Figure 8.** Division of caved zone in gob under the conditions of GERCR.

Porosity in the separation zone near the open-off cut:



https://doi.org/10.1021/acsomega.3c07755
ACS Omega 2024, 9, 3758−3771

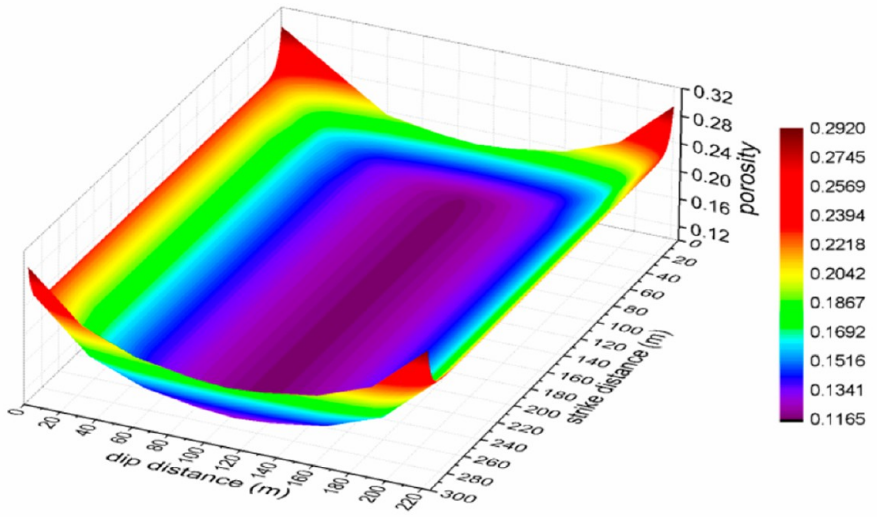


**Figure 9.** Porosity distribution in the caved zone of gob under the condition of GERCR.

$$\begin{cases} \varepsilon = (6.96434 \times 10^{-32} \times e^{(x/4.28536)} + 0.10728) + (2.20844 \times 10^{-4} \times e^{((220.2-y)/35.04021)} + 0.11178) - 0.10728, & (250.51 < x \le 295.51,\ 0 \le y < 110.1) \\ \varepsilon = (6.96434 \times 10^{-32} \times e^{(x/4.28536)} + 0.10728) + (2.20844 \times 10^{-4} \times e^{(y/35.04021)} + 0.11178) - 0.10728, & (250.51 < x \le 295.51,\ 110.1 \le y \le 220.2) \end{cases} \tag{10}$$

Porosity in the fully caved zone formed by a cutting roof:

$$\begin{cases} \varepsilon = 2.20844 \times 10^{-4} \times e^{((220.2-y)/35.04021)} + 0.11178, & (0 \le y < 110.1,\ 45 \le x \le 250.51) \\ \varepsilon = 2.20844 \times 10^{-4} \times e^{(y/35.04021)} + 0.11178, & (110.1 \le y \le 220.2,\ 45 \le x \le 250.51) \end{cases} \tag{11}$$

Porosity in the separation zone near the working face:

$$\begin{cases} \varepsilon = (6.96434 \times 10^{-32} \times e^{((295.51-x)/4.28536)} + 0.10728) + (2.20844 \times 10^{-4} \times e^{((220.2-y)/35.04021)} + 0.11178) - 0.10728, & (0 \le x < 45,\ 0 \le y < 110.1) \\ \varepsilon = (6.96434 \times 10^{-32} \times e^{((295.51-x)/4.28536)} + 0.10728) + (2.20844 \times 10^{-4} \times e^{(y/35.04021)} + 0.11178) - 0.10728, & (0 \le x < 45,\ 110.1 \le y \le 220.2) \end{cases} \tag{12}$$

A large number of studies have shown that the permeability of porous medium is not only affected by porosity but also by the direction, size, and density of fractures in the porous medium. In the caved zone, porosity varies greatly, which plays a leading role in the change of permeability. Therefore, eq 8 can be used to approximately express the relationship between porosity and permeability. In the fracture zone, the fractures are well developed, but the pores are not. Therefore, the direction, size, and density of fractures in porous medium play a leading role in the change of permeability. Compared with the caved zone, the values of permeability and porosity and their change rate are smaller in the fracture zone, and the influence on gas migration and distribution in the gob is also significantly smaller than that in the caved zone. Therefore, constant values are used to evaluate the porosity and permeability of the fracture zone. The average porosity and viscous resistance coefficient of the fracture zone were taken as 0.117 and 457753, which were the same as the values in the middle of the gob in the fully caved zone formed by the cutting roof.

The amount of gas emission from the working face and gob has an important influence on its internal flow field and is an important parameter for FLUENT simulation. Therefore, the amount of gas emission should be determined accurately. At present, the main methods to determine the gas emission in gob are the prediction of gas emission before mining and the monitoring of actual gas emission during mining. The gas emission in the gob is discharged by ventilation and drainage; therefore, it can be determined by monitoring the gas concentration and flow in the roadway and the drainage borehole. Based on the FLUENT simulation model established above, when the working face was advanced to 300 m, the gas emission from the working face and gob obtained through on-site monitoring and calculation was 1.2188 $m^3$/min and 5.31 $m^3$/min, respectively (the layout of $CH_4$ monitors are shown in Figure 15). According to the geological conditions of other coal seams adjacent to the mining #2 coal seam, as well as the characteristics of the caved zone and fracture zone in gob, it is determined that the gas emission in the caved zone accounted for 90% of the total gob gas emission, and the corresponding fracture zone accounted for 10%. Thus, in the process of


https://doi.org/10.1021/acsomega.3c07755
ACS Omega 2024, 9, 3758−3771

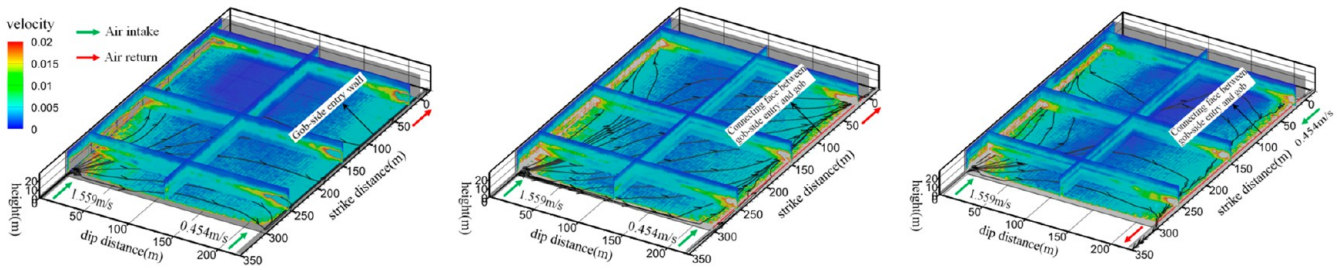


(a) Y-type ventilation under the condition of traditional gob-side entry technology (b) Y-type ventilation under the condition of GERCR technology (c) W-type ventilation under the condition of GERCR technology

**Figure 10.** (a–c) Distribution of air leakage flow field in gob under different mining and ventilation types.

FLUENT numerical simulation, the gas source terms of the working face, caved zone and fracture zone were $4.91 \times 10^{-6}$ kg/(($m^3$·s), $5.23 \times 10^{-8}$ kg/(($m^3$·s), and $8.4 \times 10^{-9}$ kg/(($m^3$·s), respectively.

**3.3. Gas Emission Characteristics.** According to the DEM-CFD model and parameters established above, the gas migration law in the gob under the conditions of GERCR technology was studied. When the interface between the gob-side entry and gob was set as a wall, the mining method was traditional gob-side entry technology, and the wall was equivalent to the supporting wall. When the interface between the gob-side entry and gob was set as the interior, the mining method was GERCR technology. Y-type and W-type ventilation are commonly used in the gob-side entry nonpillar mining technology. In the Y-type ventilation, the air entered from belt roadway and the front of track roadway with the air volume of 1.559 m/s and 0.454 m/s, respectively, and flowed out along the tail of gob-side entry. In the W-type ventilation, the air entered from belt roadway and the tail of gob-side entry with the air volume of 1.559 m/s and 0.454 m/s, respectively, and flowed out along the front of track roadway.

According to the calculation results, it can be concluded that the air leakage flow field distribution in the gob, air leakage of the working face, and air leakage of the gob-side entry under different mining and ventilation types are shown in Figure 10, Figure 11, and Figure 12, respectively. As can be seen from Figures 10–12, the air leakage in the gob under the condition of GERCR technology was essentially different from the traditional gob-side entry technology. Under the condition of

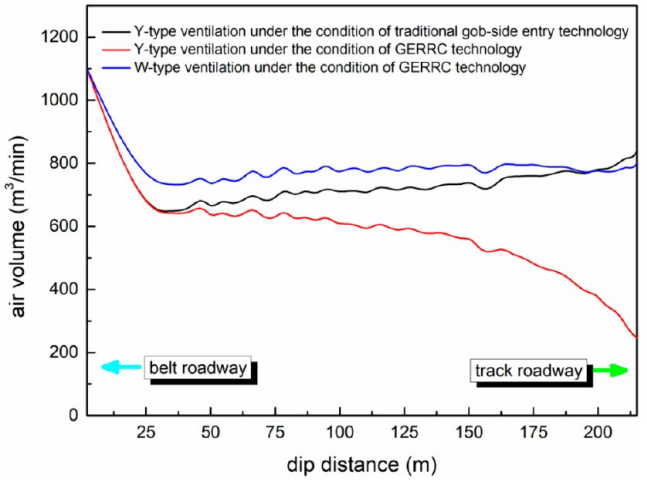


**Figure 11.** Air leakage of working face under different mining and ventilation types.

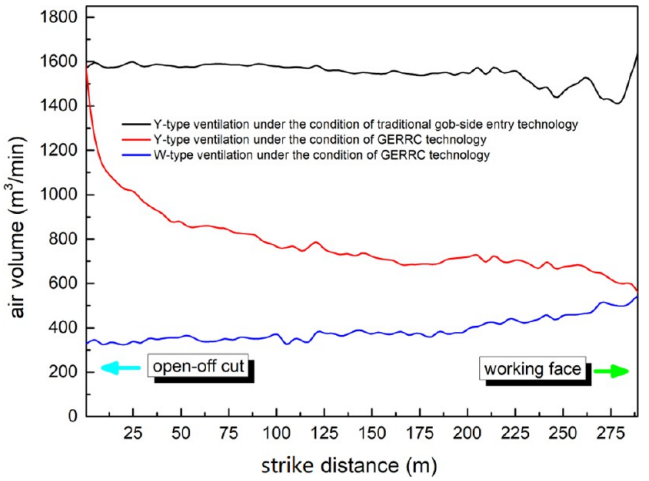


**Figure 12.** Air leakage of gob-side entry under different mining and ventilation types.

Y-type ventilation of traditional gob-side entry technology, the air flow leaked into the gob from the intersection of the belt roadway and the working face, and then flowed back to the working face. The air leakage in the working face was small. Due to the existence of the supporting wall, the air volume along the gob-side entry remained basically unchanged. Under the condition of Y-type ventilation of GERCR technology, the air leakage flow field inside the gob was penetrated, and the air flow leaked into the gob from the whole working face no longer flowed back to the working face, and the air leakage amount of the whole working face was large. Since the gob-side entry was completely connected to the caved zone of the gob, the air flow leaked into the gob from the working face continuously flowed into the gob-side entry. In the whole process of air flow in the working face, the air leakage volume was obviously segmented. The air leakage volumes at the intersection of belt roadway and working face and the intersection of track roadway and working face were large, and the air leakage volume at the middle part of the working face was relatively small. The reason can be explained by the porosity distribution in the gob, as shown in Figure 9. Under the condition of W-type ventilation of GERCR technology, the air leakage law of the gob was obviously different from the Y-type ventilation of GERCR technology. After leaking into the gob from the intersection of the belt roadway and the working face, the air flowed back to the working face. However, compared with Y-type ventilation of traditional gob-side entry technology, W-type ventilation of GERCR technology reduced the air leakage from the intersection of the belt roadway and



https://doi.org/10.1021/acsomega.3c07755
ACS Omega 2024, 9, 3758–3771

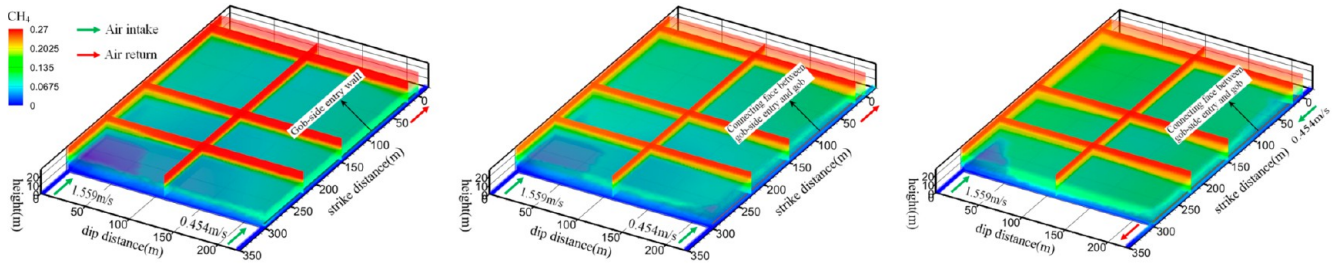


(a) Y-type ventilation under the condition of traditional gob-side entry technology (b) Y-type ventilation under the condition of GERCR technology (c) W-type ventilation under the condition of GERCR technology

**Figure 13.** (a−c) Three-dimensional distribution of gas concentration in gob under different mining and ventilation types.

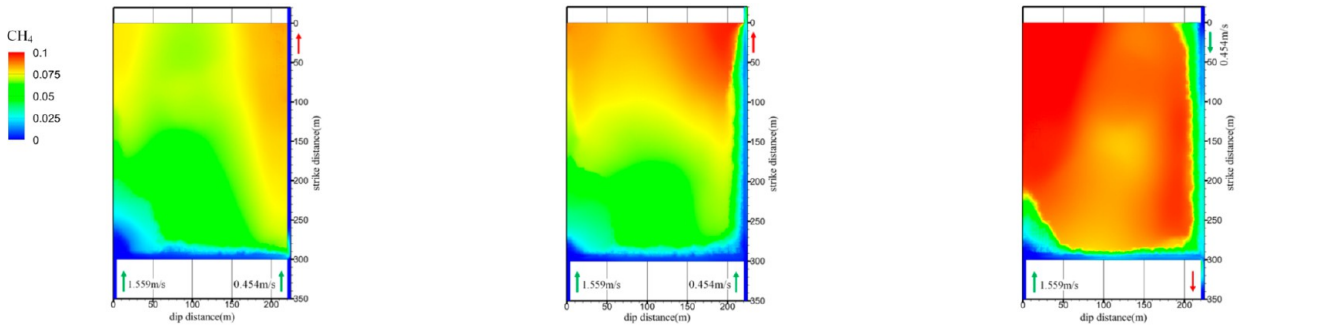


(a) Y-type ventilation under the condition of traditional gob-side entry technology (b) Y-type ventilation under the condition of GERCR technology (c) W-type ventilation under the condition of GERCR technology

**Figure 14.** (a−c) Gas concentration distribution in the plane of $z$ = 1 m in gob under different mining and ventilation types.

the working face to the gob. The main reason is that under the condition of W-type ventilation of GERCR technology, the tail of the gob-side entry was the air inlet section, where the gas pressure was obviously higher than the intersection of the belt roadway and the working face, and the pressure difference between the intersection and the inside of the gob was reduced, thereby reducing the air leakage volume.

Figure 13 and Figure 14 are the distribution of gas concentrations in three-dimensional space and $z$ = 1 m plane under different mining and ventilation types. As shown in Figure 13 and Figure 14, the change of the air leakage flow field in the gob under the condition of GERCR technology also changed the distribution and migration of gas. Due to the existence of the air leakage flow field, the gas concentrations in the deep area of the gob on the side of the belt roadway and near the working face were significantly reduced. Under the conditions of traditional gob-side entry technology, the gas concentration along the air flow in the working face increased gradually due to the gas emission from the coal wall and gob, and the highest gas concentration was near the intersection of the track roadway and the working face. In the plane of $z$ = 1 m, the gas concentration in the gob increased with the increase of the distance from the working face, and the gas concentration on the side of the belt roadway was lower than that on the track roadway side. Under the condition of Y-type ventilation of GERCR technology, the gas concentration in the working face range also increased with the air flow direction, but it was obviously reduced compared to the Y-type ventilation of traditional gob-side entry technology. The Y-type ventilation of GERCR technology was beneficial to the gas treatment of the intersection of the track roadway and the working face, which was a dangerous area of longwall mining. However, in the gob-side entry formed by GERCR technology, the gas in the gob continuously flowed into the gob-side entry, the gas concentration in the gob-side entry increased continuously with the advance of the working face, and the tail of the gob-side entry was another high gas area. That is to say, there were two high gas accumulation areas, the intersection of the track roadway and the working face and the tail of the gob-side entry. In the plane of $z$ = 1 m, the gas concentration in gob increased with the increase of the distance from the working face, and the gas concentration on the side of belt roadway was lower than that on the track roadway side. The intersection of open-off cut and gob-side entry was the area with the highest gas concentration in gob. Under the condition of W-type ventilation of GERCR technology, there was a gas dilution area at the tail of the gob-side entry. The gas concentration in the gob-side entry increased gradually from the tail to the intersection of the track roadway and the working face, which was completely opposite to the change rule of the gas concentration under the Y-type ventilation conditions of GERCR technology. Under the W-type ventilation, the gas in the roadway accumulated obviously near the intersection of the track roadway and the working face, which was the area with a serious gas disaster. In the plane of $z$ = 1 m, the deepest part of the gob on the side of the belt roadway was the area with the highest gas concentration.

## 4. CONTROL TECHNOLOGY OF GERCR GOB GAS EMISSION

As shown in Figure 14, under the condition of GERCR technology, no matter Y-type ventilation or W-type ventilation, the gas concentration in the gob was higher than that in the traditional gob-side entry technology in the plane of $z$ = 1 m, and the concentration of gas in the roadway was greater than 1%, which exceeded the limit of coal mining in China.



https://doi.org/10.1021/acsomega.3c07755
ACS Omega 2024, 9, 3758−3771

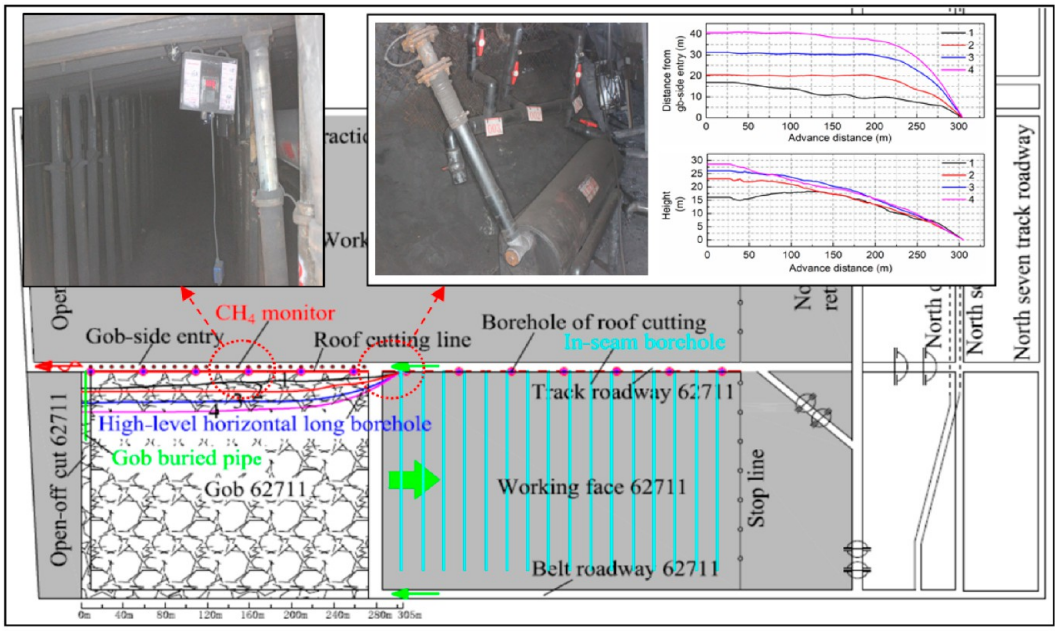


**Figure 15.** Layout of the 3D gas drainage in the GERCR working face.

Therefore, it is necessary to adopt another method to control the gas emission in gob under the conditions of GERCR technology. According to gob gas emission characteristics under the condition of GERCR technology, the technology of three-dimensional gas drainage in the GERCR working face was proposed, which included in-seam borehole drainage, high-level horizontal long borehole drainage, and gob buried pipe drainage, and the layout is shown in Figure 15. In order to control the gas emission during the mining process, in-seam boreholes were arranged in the coal seam of the working face before mining, and the coal seam gas predrainage was implemented, thereby reducing the gas content of the coal seam and the gas emission during the mining process. The length of the in-seam borehole was 200 m, the diameter was 113 mm, the spacing was 10 m, and the borehole was perpendicular to the coal seam face in the roadway. In the track roadway 62711, the high-level horizontal long boreholes were arranged by using directional drilling equipment and technology so as to extract the gas accumulated in the fracture zone and reduce the gas emission in the gob. In order to maximize gas drainage, the spatial coordinates of the high-level horizontal long boreholes were determined according to the PFC simulation results. Four rectangular drilling fields with a length of 7 m and a depth of 3 m were arranged in the whole working face, and the spatial distribution of the four boreholes in the first drilling field is shown in Figure 15. In addition, according to the above FLUENT simulation results, the gas concentration was high in the deep gob near the open-off cut; therefore, the pipe was buried at this position for gas drainage.

In order to further determine the characteristics of gas emission and the control effect of the three-dimensional drainage in gob, 192 days of continuous observation were carried out on the GERCR working face 62711 of the Duerping coal mine since February 25, 2017. During this period, the working face was advanced to 530 m. The changes of ventilation types and air volume of the working face during the 0−530 m advance process are shown in Figure 16. 0−408 m, the ventilation was Y-type; 408−530 m, the ventilation changed to W-type. In the Y-type ventilation, the air entered

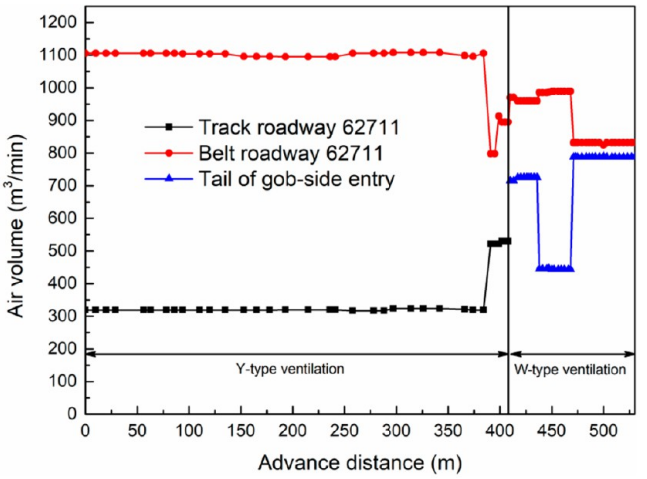


**Figure 16.** Change of ventilation types and air volume of the working face during the 0−530 m advance process.

from the belt roadway and the front of the track roadway and flowed out along the tail of the gob-side entry. In the W-type ventilation, the air entered from the belt roadway and the tail of the gob-side entry and flowed out along the front of the track roadway. In order to monitor the gas emission in gob, with the advance of the working face, a $CH_4$ monitor was arranged every 10 m along the gob-side entry (the $x$ coordinate of the open-off cut was 0 m), and the layout of the $CH_4$ monitor is shown in Figure 15. Through 192 days of on-site monitoring, the change of gas emission volume in the GERCR working face is shown in Figure 17, and the change law of gas concentration at different positions along the gob-side entry with the advance distance is shown in Figure 18. As shown in Figure 17, when the three-dimensional drainage system designed above was used for gas drainage, the gas drainage volume was maintained at about 5 $m^3$/min, the drainage effect was significant, and the drainage volume was stable. The drainage volume was less affected by the advance distance and ventilation type of the working face. Under the condition of Y-


https://doi.org/10.1021/acsomega.3c07755
ACS Omega 2024, 9, 3758−3771

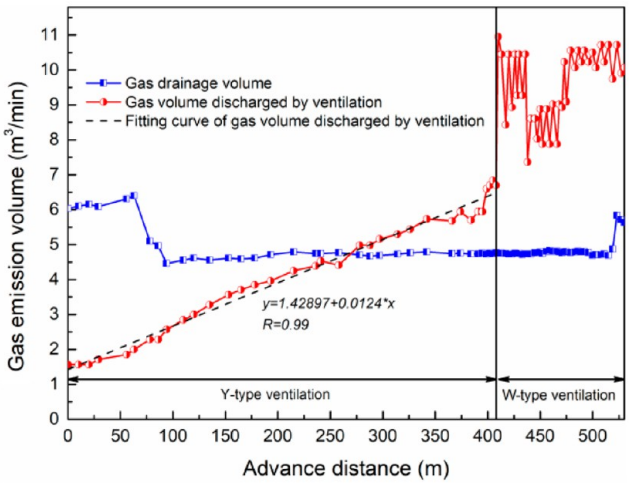


**Figure 17.** Change of gas emission volume in the GERCR working face.

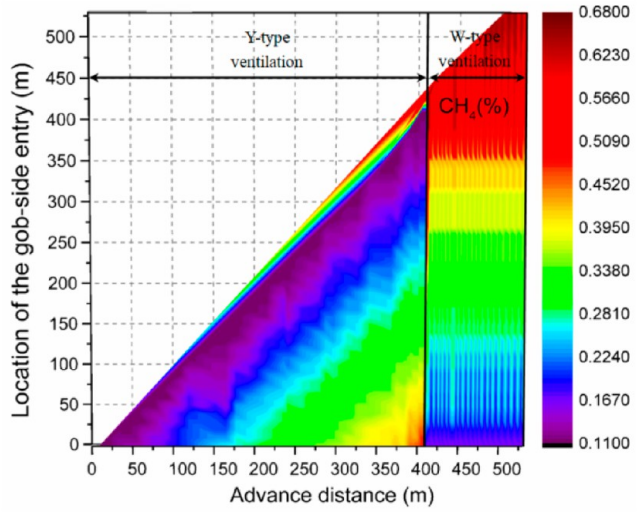


**Figure 18.** Change of gas concentration at different positions along the gob-side entry with the advance distance.

type ventilation (0−408 m), the gas discharged by ventilation increased with the increase of advance distance, and the relationship between them was in good accordance with the linear relationship of equation $y = 1.42897 + 0.0124x$. Under the condition of W-type ventilation (408−530 m), due to the large fluctuation of air intake volume, the relationship between the gas discharged by ventilation and the advance distance was not significant. In the mining process of GERCR technology, the indication of the gas monitors arranged along the gob-side entry in Figure 15 changed continuously with an increase of advance distance. When the working face was advanced to different positions, the relationship between the gas concentration at different positions of the gob-side entry and the advance distance was fitted, and the spatiotemporal change rule of the gas concentration at different positions of the gob-side entry is shown in Figure 18. During the 0−408 m advance process (Y-type ventilation), with the increase of advance distance, the gas concentration at different positions of the gob-side entry gradually increased; when the advance distance was fixed, the gas concentration in the gob-side entry decreased with the increase of the position value. During the 408−530 m advance process (W-type ventilation), with the increase of advance distance, the gas concentration at different positions of the gob-side entry remained unchanged; when the advance distance was fixed, the gas concentration at different positions of the gob-side entry increased with the increase of the position value. Under the conditions of Y-type ventilation and W-type ventilation, the gas concentration distribution rule in the gob-side entry was basically consistent with the above numerical simulation results, and the gas concentration in the whole mining process did not exceed 1%. The on-site monitoring results show that the DEM-CFD coupled model established above can well simulate the gas emission characteristics of the GERCR gob and the three-dimensional drainage system can well control the gas concentration in the roadway.

## 5. CONCLUSIONS

Under the conditions of GERCR technology, the overburden collapse and fracture development in gob are obviously different from that under the traditional mining conditions. The cutting of the basic roof made the basic roof and the overburden under its control fully collapse, and the height of the caved zone in the gob increased obviously. In the range from the upper part of the coal seam to the basic roof, the development degree of fracture on the roof cutting side was higher; in the range from the upper part of the basic roof to the main key layer, the development degree of fracture on the roof not cutting side was higher. The area where the overburden porosity increased significantly on the roof cutting side was smaller than that on the roof not cutting side, and the influence area of the roadway side support was more unfavorable to the gas flow.

Under the conditions of GERCR technology, the gas emission characteristics in gob are obviously different from that under the traditional mining conditions. Under the condition of Y-type ventilation of GERCR technology, the gas concentration in the working face range increased with the air flow direction but was obviously reduced compared with the Y-type ventilation of traditional gob-side entry technology. The Y-type ventilation of the GERCR technology was beneficial to the gas treatment of the intersection of the track roadway and the working face. However, in the gob-side entry formed by GERCR technology, the gas in the gob continuously flowed into the gob-side entry, and the gas concentration in the gob-side entry increased continuously with the advance of the working face, and the tail of gob-side entry was another high gas area. Under the condition of W-type ventilation of GERCR technology, there was a gas dilution area at the tail of gob-side entry. The gas concentration in the gob-side entry increased gradually from the tail to the intersection of the track roadway and the working face, which was completely opposite the change rule of the gas concentration under the Y-type ventilation condition. Under the W-type ventilation, the gas in the roadway accumulated obviously near the intersection of the track roadway and the working face, which was the area with serious gas disaster.

When the designed three-dimensional drainage system was used for gas drainage, the gas drainage volume was maintained at about 5 $m^3$/min, the drainage effect was significant, and the drainage volume was stable. The drainage volume was less affected by the advance distance and ventilation type of the working face. Under the condition of Y-type ventilation, the gas discharged by ventilation increased with the increase of


https://doi.org/10.1021/acsomega.3c07755
ACS Omega 2024, 9, 3758−3771

advance distance, and the relationship between them was in good accordance with the linear relationship. The on-site monitoring results show that the DEM-CFD coupled model established above can well simulate the gas emission characteristics of the GERCR gob, and the three-dimensional drainage system can well control the gas concentration in the roadway.

## AUTHOR INFORMATION


### Corresponding Author

**Hongwei Liu** − *College of Safety and Emergency Management Engineering, Taiyuan University of Technology, Taiyuan 030024, China; School of Civil, Mining and Environmental Engineering, University of Wollongong, Wollongong, New South Wales 2500, Australia;* orcid.org/0000-0003-2943-5553; Email: liuhongwei01@tyut.edu.cn

### Authors

**Xu Zheng** − *College of Safety and Emergency Management Engineering, Taiyuan University of Technology, Taiyuan 030024, China;* orcid.org/0009-0004-5056-8267

**Shaocheng Ge** − *College of Safety and Emergency Management Engineering, Taiyuan University of Technology, Taiyuan 030024, China;* orcid.org/0000-0001-7398-9102

**Jia Liu** − *College of Safety and Emergency Management Engineering, Taiyuan University of Technology, Taiyuan 030024, China*

**Jingjing Yan** − *College of Safety and Emergency Management Engineering, Taiyuan University of Technology, Taiyuan 030024, China; School of Energy Industry, Shanxi College of Technology, Shuozhou 036000, China;* orcid.org/0000-0002-5562-0181

Complete contact information is available at: https://pubs.acs.org/10.1021/acsomega.3c07755


### Notes

The authors declare no competing financial interest.

## ACKNOWLEDGMENTS

This work was supported by the National Natural Science Foundation of China (No. 52304246); the Research Project Supported by Shanxi Scholarship Council of China (No. 2023-057); the Basic Research Program (Free Exploration) Project of Shanxi Province (No. 20210302124222); the Higher Education Science and Technology Innovation Project of Shanxi Province (No. 2021L050); the School Fund Project of Taiyuan University of Technology (No. 2022QN136); and China Scholarship Council (No. 201806930016).

## REFERENCES


(1) Wang, M.; Xu, Y. L.; Xu, Q. Y.; Shan, C. F.; Li, Z. H.; Nan, H.; Li, Y. F.; Liu, H. L.; Chu, T. X. Stability control of overburden and coal pillars in the gob-side entry under dynamic pressure. *Int. J. Rock Mech. Min. Sci.* **2023**, *170*, 105490.

(2) Wang, P.; Jiang, L.; Jiang, J.; Zheng, P.; Li, W. Strata Behaviors and Rock Burst-Inducing Mechanism under the Coupling Effect of a Hard, Thick Stratum and a Normal Fault. *International Journal of Geomechanics* **2018**, *18* (2), 04017135.

(3) Zhang, Z.; Shimada, H.; Sasaoka, T.; Hamanaka, A. Stability Control of Retained Goaf-Side Gateroad under Different Roof Conditions in Deep Underground Y Type Longwall Mining. *Sustainability* **2017**, *9* (10), 1671.

(4) Ma, Q.; Tan, Y. L.; Zhao, Z. H.; Xu, Q.; Wang, J.; Ding, K. Roadside support schemes numerical simulation and field monitoring of gob-side entry retaining in soft floor and hard roof. *Arabian Journal of Geosciences* **2018**, *11* (18), 563.

(5) Meng, X. R.; Peng, R.; Zhao, G. M.; Li, Y. M. Roadway Engineering Mechanical Properties and Roadway Structural Instability Mechanisms in Deep Wells. *Ksce Journal of Civil Engineering* **2018**, *22* (5), 1954−1966.

(6) Chen, S. J.; Qu, X.; Yin, D. W.; Liu, X. Q.; Ma, H. F.; Wang, H. Y. Investigation lateral deformation and failure characteristics of strip coal pillar in deep mining. *Geomechanics and Engineering* **2018**, *14* (5), 421−428.

(7) Huang, W. P.; Yuan, Q.; Tan, Y. L.; Wang, J.; Liu, G. L.; Qu, G. L.; Li, C. An innovative support technology employing a concrete-filled steel tubular structure for a 1000-m-deep roadway in a high in situ stress field. *Tunnelling and Underground Space Technology* **2018**, *73*, 26−36.

(8) Ning, J. G.; Liu, X. S.; Tan, J.; Gu, Q. H.; Tan, Y. L.; Wang, J. Control mechanisms and design for a 'coal-backfill-gangue' support system for coal mine gob-side entry retaining. *International Journal of Oil Gas and Coal Technology* **2018**, *18* (3/4), 444−466.

(9) Gong, P.; Ma, Z. G.; Ni, X. Y.; Zhang, R. R. An Experimental Investigation on the Mechanical Properties of Gangue Concrete as a Roadside Support Body Material for Backfilling Gob-Side Entry Retaining. *Advances in Materials Science and Engineering* **2018**, *2018*, 1−11.

(10) He, M.; Zhu, G.; Guo, Z. Longwall mining"cutting cantilever beam theory"and 110 mining method in ChinadThe third mining science innovation. *Journal of Rock Mechanics and Geotechnical Engineering* **2015**, *7* (5), 483−492.

(11) Tao, Z.; Song, Z.; He, M.; Meng, Z.; Pang, S. Principles of the roof cut short-arm beam mining method (110 method) and its mining-induced stress distribution. *International Journal of Mining Science and Technology* **2018**, *28* (3), 391−396.

(12) Tu, Q. Y.; Cheng, Y. P.; Xue, S.; Ren, T.; Cheng, X. Energy-limiting factor for coal and gas outburst occurrence in intact coal seam. *International Journal of Mining Science and Technology* **2021**, *31* (4), 729−742.

(13) Liu, H.; Wang, F.; Ren, T. Research on the characteristics of the coal-oxygen reaction in a lean-oxygen environment caused by methane. *Energy Fuels* **2019**, *33* (9), 9215−9223.

(14) Liu, H.; Wang, F.; Ren, T.; Qiao, M.; Yan, J. Influence of methane on the prediction index gases of coal spontaneous combustion: A case study in Xishan coalfield, China. *Fuel* **2021**, *289*, 119852.

(15) Chen, X.; Li, L.; Wang, L.; Qi, L. The current situation and prevention and control countermeasures for typical dynamic disasters in kilometer-deep mines in China. *Safety Science* **2019**, *115*, 229−236.

(16) Zhou, F.; Xia, T.; Wang, X.; Zhang, Y.; Sun, Y.; Liu, J. Recent developments in coal mine methane extraction and utilization in China: A review. *Journal of Natural Gas Science and Engineering* **2016**, *31*, 437−458.

(17) Karakurt, I.; Aydin, G.; Aydiner, K. Mine ventilation air methane as a sustainable energy source. *Renewable & Sustainable Energy Reviews* **2011**, *15* (2), 1042−1049.

(18) Baris, K. Assessing ventilation air methane (VAM) mitigation and utilization opportunities: A case study at Kozlu Mine, Turkey. *Energy for Sustainable Development* **2013**, *17* (1), 13−23.

(19) Lin, J.; Ren, T.; Wang, G.; Booth, P.; Nemcik, J. Experimental investigation of $N_2$ injection to enhance gas drainage in CO2-rich low permeable seam. *Fuel* **2018**, *215*, 665−674.

(20) Lin, J.; Ren, T.; Cheng, Y.; Nemcik, J.; Wang, G. Cyclic $N_2$ injection for enhanced coal seam gas recovery: A laboratory study. *Energy* **2019**, *188*, 116115.

(21) Li, X.; Wang, C.; Chen, Y.; Tang, J.; Li, Y. Design of gas drainage modes based on gas emission rate in a gob: a simulation study. *Arabian Journal of Geosciences* **2018**, *11* (16), 456.

(22) Si, G.; Belle, B. Performance analysis of vertical goaf gas drainage holes using gas indicators in Australian coal mines. *International Journal of Coal Geology* **2019**, *216*, 103301.
(23) Tanguturi, K.; Balusu, R. Fundamental understanding of goaf gas displacement in longwall goaf. *Journal of Mining and Environment* **2015**, *6* (2), 191−203.
(24) Tanguturi, K.; Balusu, R. Computational fluid dynamics simulations for investigation of parameters affecting goaf gas distribution. *Journal of Mining and Environment* **2018**, *9* (3), 547−557.
(25) Qin, Z.; Yuan, L.; Guo, H.; Qu, Q. Investigation of longwall goaf gas flows and borehole drainage performance by CFD simulation. *International Journal of Coal Geology* **2015**, *150*, 51−63.
(26) Guo, H.; Todhunter, C.; Qu, Q.; Qin, Z. Longwall horizontal gas drainage through goaf pressure control. *International Journal of Coal Geology* **2015**, *150*, 276−286.
(27) Ren, T.; Wang, Z. Computational fluid dynamics modelling of respirable dust and gas behaviour on a longwall face. *Int. J. Biochem. Cell Biol.* **2013**, *45* (9), 1962−1973.
(28) Wang, Z.; Ren, T.; Cheng, Y. Numerical investigations of methane flow characteristics on a longwall face Part II: Parametric studies. *Journal of Natural Gas Science and Engineering* **2017**, *43*, 254−267.
(29) Majdi, A.; Hassani, F. P.; Nasiri, M. Y. Prediction of the height of destressed zone above the mined panel roof in longwall coal mining. *International Journal of Coal Geology* **2012**, *98*, 62−72.
(30) Ozgen Karacan, C.; Goodman, G. V.R. Probabilistic modeling using bivariate normal distributions for identification of flow and displacement intervals in longwall overburden. *Int. J. Rock Mech. Min. Sci.* **2011**, *48* (1), 27−41.
(31) Peng, S.; Chiang, H. *Longwall Mining*; John Wiley and Sons; New York, Brisbane, Toronto Singapore, 1984.
(32) Karacan, C. O.; Esterhuizen, G. S.; Schatzel, S. J.; Diamond, W. P. Reservoir simulation-based modeling for characterizing longwall methane emissions and gob gas venthole production. *International Journal of Coal Geology* **2007**, *71* (2−3), 225−245.
(33) Guo, H.; Yuan, L.; Shen, B.; Qu, Q.; Xue, J. Mining-induced strata stress changes, fractures and gas flow dynamics in multi-seam longwall mining. *International Journal of Rock Mechanics & Mining Sciences* **2012**, *54*, 129−139.
(34) Qian, M.; Xu, J. Study on the "O shape" circle distribution characteristics of mining induced fractures in the overlaying strata. *Journal of China Coal Society* **1998**, *23* (5), 466−469.
(35) Guo, H.; Qin, J.; Qu, Q. CFD Investigation of goaf flow of methane released from unmined adjacent coal seams, Ninth International Conference on CFD in the Minerals and Process Industries, CSIRO, Melbourne, Australia, December 10-12, 2012. *Melbourne* **2012**, 1−6.
(36) Rezaei, M. Development of an intelligent model to estimate the height of caving-fracturing zone over the longwall gobs. *Neural Computing and Applications* **2018**, *30* (7), 2145−2158.
(37) Rezaei, M.; Hossaini, M. F.; Majdi, A. A time-independent energy model to determine the height of destressed zone above the mined panel in longwall coal mining. *Tunnelling and Underground Space Technology* **2015**, *47*, 81−92.
(38) Wang, G.; Fan, C.; Xu, H.; Liu, X.; Wang, R. Determination of Long Horizontal Borehole Height in Roofs and Its Application to Gas Drainage. *Energies* **2018**, *11* (10), 2647.
(39) Whittles, D.; Lowndes, I.; Kingman, S.; Yates, C.; Jobling, S. Influence of geotechnical factors on gas flow experienced in a UK longwall coal mine panel. *Int. J. Rock Mech. Min. Sci.* **2006**, *43* (3), 369−387.
(40) Cui, F.; Jia, C.; Lai, X. Study on deformation and energy release characteristics of overlying strata under different mining sequence in close coal seam group based on similar material simulation. *Energies* **2019**, *12* (23), 4485.
(41) Wang, X.; Qin, Q.; Fan, C. Failure characteristic and fracture evolution law of overburden of thick coal in fully mechanized sub-level caving mining. *JSM* **2017**, *46* (11), 2041−2048.
(42) Liu, H.; Liu, S.; Chen, L.; Jia, G.; Wang, F.; Li, Z.; Yan, J. Distribution characteristics of spontaneous combustion zone and spray plugging fire prevention and extinguishing technology in goaf of roof cutting and gob-side entry retaining. *J. Min. Saf. Eng.* **2022**, *39* (3), 624−633 (in Chinese).
(43) Cundall, P. A.; Strack, O. D. A discrete numerical model for granular assemblies. *geotechnique* **1979**, *29* (1), 47−65.
(44) Zou, Z.; Tang, H.; Xiong, C.; Su, A.; Criss, R. E. Kinetic characteristics of debris flows as exemplified by field investigations and discrete element simulation of the catastrophic Jiweishan rockslide, China. *Geomorphology* **2017**, *295*, 1−15.
(45) Wang, T.; Zhou, W.; Chen, J.; Xiao, X.; Li, Y.; Zhao, X. Simulation of hydraulic fracturing using particle flow method and application in a coal mine. *International Journal of Coal Geology* **2014**, *121*, 1−13.
(46) Liu, H.; Zhao, Y.; Ren, T.; Wang, F.; Li, Z. Characteristics of overburden failure and fracture development in gob of mining with gob-side entry formed by cutting roof. *Journal of China University of Mining & Technology* **2022**, *51* (1), 77−89 (in Chinese).
(47) Cho, N. a.; Martin, C.; Sego, D. A clumped particle model for rock. *Int. J. Rock Mech. Min. Sci.* **2007**, *44* (7), 997−1010.
(48) Potyondy, D. O.; Cundall, P. A bonded-particle model for rock. *Int. J. Rock Mech. Min. Sci.* **2004**, *41* (8), 1329−1364.
(49) Wang, X.; Qin, Q.; Fan, C. Failure characteristic and fracture evolution law of overburden of thick coal in fully mechanized sub-level caving mining. *JSM***2017**, *46* (11), 2041−2048.
(50) Qian, M.; Shi, P. *Ground Pressure and Strata Control*; China University of Mining and Technology Press: Xuzhou, 2003. (in Chinese).



https://doi.org/10.1021/acsomega.3c07755
*ACS Omega* 2024, 9, 3758−3771